Atmos. Chem. Phys. Discuss., 12, 15301–15335, 2012
www.atmos-chem-phys-discuss.net/12/15301/2012/
doi:10.5194/acpd-12-15301-2012

Atmospheric Chemistry and Physics Discussions

Characterization of Eyjafjallajökull volcanic aerosols over Southeastern Italy

M. R. Perrone[1], **F. De Tomasi**[1], **A. Stohl**[2], **and N. I. Kristiansen**[2]

[1]Physics Department, University of Salento, Lecce, Italy
[2]NILU-Norwegian Institute for Air Research, Kjeller, Norway

Received: 21 May 2012 – Accepted: 4 June 2012 – Published: 15 June 2012

Correspondence to: M. R. Perrone (perrone@le.infn.it)

Published by Copernicus Publications on behalf of the European Geosciences Union.

Abstract

Volcanic aerosols resulting from the Eyjafjallajökull eruption have been detected in Southeastern Italy from 20 to 22 April 2010, at a distance of approximately 4000 km from the volcano site, and have been characterized by lidar, sun/sky photometer, and in-situ measurements. Numerical simulations by the FLEXPART dispersion model, meteorological synoptic maps, and analytical backtrajectories confirm the advection of volcanic aerosols to the monitoring site. However, both the peak concentrations as well as the total column loadings of volcanic ash simulated by FLEXPART were about one order of magnitude lower than corresponding values simulated over Central Europe on 16 April. This suggests that the volcanic ash over Southeastern Italy was strongly diluted. Nevertheless, volcanic particles added to the pre-existing aerosol load and the integrated use of FLEXPART simulations and experimental measurements has allowed to clearly identifying the impact of volcanic particles on the aerosol vertical distribution, the aerosol size distribution, and the ground-level particulate-matter concentrations. Lidar measurements performed at the Physics Department of the University of Salento (40.4° N; 18.1° E) within EARLINET (European Aerosol Research LIdar NETwork EARLINET) have revealed the first arrival of volcanic aerosols on the afternoon of 20 April. In particular, lidar measurements have shown that at 18:30 UTC of 20 April, lidar ratios (LRs) at 355 nm varied from 65 to 71 sr inside the volcanic aerosol layer located between 2.5–3.5 km from the ground level and were characterized by smaller values (≅45 sr) in the underlying layer. The LR dependence on altitude has decreased with time as volcanic particles also reached ground level. Then, LRs varied between 41 and 60 sr all over the aerosol column at 02:30 UTC of 21 April. The time evolution of the aerosol optical depth from lidar measurements was similar to that of the ash-total-column mass concentration from FLEXPART simulations after midday of 21 April, for the larger contribution of volcanic particles to the whole aerosol load. Sun/sky photometer measurements performed within AERONET, have revealed that the mass size distribution of volcanic particles retrieved from measurements performed on 21 April

ACPD

12, 15301–15335, 2012

was in reasonable accordance with the volcanic-ash mass size distribution from FLEXPART simulations. Volcanic particles with radius $r > 0.5\,\mu m$ have mainly been advected over Southeastern Italy and the contribution of coarse volcanic particles has increased from 20 to 22 April. The aerosol fine mode fraction from sun-sky photometer measurements varied between 0.85 and 0.94 on 20 April, but decreased to values between 0.25 and 0.82 on 22 April. Surface measurements of particle size distributions have also supported the advection of coarse volcanic particles. More specifically, mass concentrations of daily PM_1 and $PM_{2.5}$ samples revealed that the $PM_1/PM_{2.5}$ mass ratios were 0.69, 0.66, and 0.60 on 20, 21, and 22 April, respectively, indicating an increasing fraction of super-micron particles. Finally, measurements from the Regional Air Quality Agency have revealed enhanced PM_{10} and SO_2 mass concentrations on 20, 21 and/or 22 April, 2010 all over the ~400 km long Apulia Region. The estimated enhancement of PM_{10} from volcanic particles was ~6 $\mu g\,m^{-3}$ on 21 April at the monitoring site of this study, in satisfactory accordance with FLEXPART simulations.

1 Introduction

The eruption of the Eyjafjallajökull volcano in Iceland entered a strong phase of ejection of ash to the atmosphere on 14 April 2010, which lasted for several days. In the initial explosive phase, the eruption ejected volcanic ash to altitudes as high as 10 km a.s.l., as reported by the Institute of Earth Sciences (IES, www.earthice.hi.is). The westerly winds over Iceland transported the volcanic emissions first toward Northern Europe (starting with UK and Norway) (Petersen, 2010) and then, towards Central and Southern Europe. Emeis et al. (2011) found from remote sensing data and numerical simulations that the first volcanic ash layer reached Germany on 16 April. The volcanic aerosol plume was detected in clear layers above Switzerland starting from 17 April (Bukowiecki et al., 2011), above Southern Italy from 19 April (Madonna et al., 2010; Mona et al., 2012), and over Greece after 21 April (Papayannis et al., 2012). The volcano's initially explosive activity decreased continuously to a more effusive

ACPD
12, 15301–15335, 2012

eruption a few days after (Kristiansen et al., 2012). The explosive activity increased again around 5 May and it ended around 23 May 2010. Minor volcanic activity was observed until middle of June 2010 (Langmann et al., 2012). The space-time evolution of the distribution of the volcanic plume over Europe has been investigated extensively by EARLINET, the European Aerosol Research LIdar NETwork, which performed almost continuous measurements from 15 April to 22 May 2010 (e.g., Ansmann et al., 2010; Mona et al., 2012; Papayannis et al., 2012). Lidar instruments are well suited to observe aerosol layers in higher altitudes and to provide information about their vertical structure and development with time. In addition to lidars, different ground-based, airborne and space-borne instruments have been used to characterize the physical and optical properties of the volcanic aerosols resulting from the Eyjfjallajökull eruption (e.g., Bukowiecki et al., 2011; Revuelta et al., 2012; Campanelli et al., 2012; Schumann et al., 2011; Toledano et al., 2012; Rossini et al., 2012).

This paper focuses on the characterization of aged volcanic aerosols detected from 20 to 22 April 2010 at Lecce (40.4° N; 18.1° E), in Southeastern Italy, approximately 4000 km away from the Eyjafjallajökull volcano. After advection over several thousand of kilometres, volcanic ash surfaces can be modified by condensation and coagulation processes upon contact with atmospheric trace gases and aerosols (Langmann et al., 2012) and are highly dispersed. Their microphysical and optical properties which may have changed during advection are not well known and hence, are especially interesting to study. Aerosol observations performed thousands of kilometres away from source regions are also important for the validation of volcanic ash transport models. The use of different remote sensing and in-situ sampling devices to characterize aged volcanic particles represents the main objective of this study. More specifically, lidar measurements performed within EARLINET have been used to characterize the evolution in space and time of the aerosol load during the advection of volcanic particles. Sun/sky photometer measurements performed within AERONET (Holben et al., 1998) at the lidar site, have been used to infer volcanic aerosol effects on the main column-averaged aerosol optical and microphysical properties. In-situ

ACPD
12, 15301–15335, 2012

measurements have been performed to characterize the size distribution of ground particles and to monitor the mass concentration of PM_1 and $PM_{2.5}$ particles. Finally, in-situ SO_2 and PM_{10} measurements performed by the Regional Air Quality Agency (www.arpa.puglia.it/web/guest/qariainq) have been analyzed to study the impact of volcanic aerosols on regional air quality.

Synoptic meteorological maps, analytical back trajectories and numerical simulations with the dispersion model FLEXPART (Stohl et al., 2005) have been used to confirm the advection of volcanic aerosols to the monitoring site. An overview of the instrumentation and a brief description of the FLEXPART dispersion model are given in Sect. 2. Results and discussion are reported in Sect. 3. Main conclusions and caveats are presented in Sect. 4.

2 Instrumentation and FLEXPART model

2.1 Experimental devices

Remote sensing and in-situ measurements were conducted at the Physics Department of the University of Salento (40.4° N; 18.1° E) which is located 6 km away from the town of Lecce, in Southeastern Italy, and approximately 4000 km away from Iceland.

Lidar measurements are regularly performed at the Physics Department with a Raman lidar identified as UNILE (UNIversity of LEcce) lidar. The ground-based Raman lidar, that is operative since the beginning of the European Aerosol Research LIdar NETwork (EARLINET) in May 2000 (Matthias et al., 2004), nowadays employs an f/4 Newton telescope with a 30-cm-diameter mirror and a frequency-tripled Nd-YAG laser (355 nm) that delivers pulses of ~350 mJ of energy at a repetition rate of 30 Hz. The UNILE-lidar has been designed to derive at 355 nm vertical profiles of aerosol extinction ($\alpha(z)$) and backscatter ($\beta(z)$) coefficients and lidar ratios (LR(z)) during night time and to retrieve aerosol backscatter vertical profiles during day time measurements. Details on experimental apparatus and data analysis are reported in De Tomasi and

ACPD
12, 15301–15335, 2012

Perrone (2003) and De Tomasi et al. (2003, 2006). The statistical uncertainties of $\beta(z)$ are calculated from the error propagation law by assuming a Poisson noise on the lidar signals. The aerosol extinction coefficient is calculated by a linear fit of the derivative of the logarithm of the nitrogen Raman signal with respect to the range (Ansmann et al., 1992) and its uncertainties are set as the uncertainties associated to the slope of the fitting straight lines. Lidar ratio ($LR(z) = \alpha(z)/\beta(z)$) uncertainties are calculated using standard propagation techniques (Bevington and Robinson, 2003). The lidar system is estimated to achieve full overlap between 0.3–0.5 km (Matthias et al., 2004).

An AERONET sun/sky radiometer operates at the lidar site since March 2003. AERONET is a federated international network of sun/sky radiometers established in 1993 (Holben et al., 1998). Data are publicly available online in near real-time mode (http://aeronet.gsfc.nasa.gov). The sun/sky radiometer measures direct sun radiance in eight spectral channels between 340 and 1020 nm (340, 380, 440, 500, 670, 870, 940 and 1020 nm). Sky measurements are performed at 440, 670, 870 and 1020 nm wavelengths through a wide range of scattering angles from the Sun (Holben et al., 1998). An automated cloud-screening algorithm (Smirnov et al., 2000) is applied to AOD direct-sun measurements. Aerosol microphysical parameters are retrieved from direct sun and diffuse sky radiance measurements by a flexible inversion algorithm, developed by Dubovik and King (2000). A discussion on the accuracy of individual retrievals is reported in Dubovik et al. (2000). Quality assured (automatically cloud cleared and manually inspected) level 2 AERONET data retrieved from measurements performed between 19 and 22 April 2010 have been used in this study.

For continuous size distribution measurements at about 10 m from the ground, a TSI Aerodynamic Particle Sizer (APS) 3321 with 51 channels of equal logarithmic width of 0.031 within the diameter size range of 0.54–20.0 µm, was deployed. The APS measurements started on 21 April at midday. Particulate matter (PM) samples have also been collected at ∼10 m a.g.l. with a low volume (2.3 $m^3 h^{-1}$) HYDRA-FAI dual sampler which allowed to simultaneously collect 24-h $PM_{2.5}$ and PM_1 samples on 47-mm-diameter preheated filters (PALLFLEX, Tissuquartz). The filters were conditioned for

ACPD
12, 15301–15335, 2012

48 h (25 °C and 50 % humidity) before and after sampling and PM mass concentrations have been determined by the gravimetric method. Uncertainties on mass concentrations are lower than 5 %.

2.2 The FLEXPART dispersion model

The Lagrangian particle dispersion model FLEXPART (Stohl et al., 1998, 2005) was used to simulate the transport of volcanic ash. FLEXPART was run in forward mode and driven with meteorological data from the European Centre for Medium-Range Weather Forecasts (ECMWF) analyses with 0.18° × 0.18° horizontal resolution and 91 vertical model levels. The simulation accounted for gravitational particle settling as well as dry and wet deposition, but not for ash aggregation processes. Formation of sulphate particles was also not simulated. Ash emission rates as a function of time and height, determined previously using an inversion scheme that coupled a priori source information and FLEXPART model results with satellite data (Stohl et al., 2011), were used as a source term for this study. The ash particle size distribution included 25 particle size classes from 0.25–250 µm diameter. The model output had a horizontal resolution of 0.25° × 0.25° and a vertical resolution of 250 m.

3 Results and discussion

3.1 Methodology to detect the advection of volcanic aerosols

The height of the eruption cloud which varied from about 3 km up to 10 km and the prevailing mid-tropospheric west-north-westerly winds over the Eastern North Atlantic north of the British Isles carried the volcanic aerosol first across Northwestern and then Central Europe. More specifically, the synoptic meteorological situation on 14–15 April, with a high located South of Iceland and a trough over Northern Scandinavia, favoured the transport of ash first over Norway and later over Southern England, Denmark and

ACPD
12, 15301–15335, 2012

Central Europe (e.g., Peterson, 2010; Folch et al., 2012). Stagnant conditions over Central Europe during the following days favored a long residence time of the ash over Europe, associated with slow subsidence of the ash layers and settling of larger particles. The situation changed on 20 April when northwesterly winds transported parts of the volcanic ash plume first over South-Southeastern Europe and then over Eastern Europe on 23 April (Fig. 1 of the paper by Folch et al., 2012). Eight-day analytical back trajectories from the Hybrid Single Particle Lagrangian Integrated Trajectory Model (HYSPLIT) (Draxler and Rolph, 2010) show that air masses arriving over Lecce on 20 (Fig. 1a), 21 (Fig. 1b, c) and 22 April (Fig. 1d) had previously travelled across Iceland. Plots of volcanic-ash column-integrated mass concentrations from FLEXPART (Fig. 2) also reveal the advection of volcanic aerosol over Southeastern Italy from 20 to 22 April. The green dot in Fig. 2 represents the lidar site. In particular, we observe that ash columnar mass concentrations at Lecce are higher than a few $\mathrm{mg\,m^{-2}}$ after the afternoon of 20 April. They reach the highest values of nearly $200\,\mathrm{mg\,m^{-2}}$ during the night of 20/21 April and subsequently decrease to rather low levels in the afternoon of 22 April. However, notice that even the largest ash column loadings over Lecce are about one order of magnitude lower compared to those simulated by FLEXPART over Central Europe on 16 April (Stohl et al., 2011). Thus, while some volcanic ash reached Southeastern Italy, it is much more diluted than earlier over Central Europe and, thus, mixing with aerosols from other sources is likely to be relatively important.

3.2 UNILE lidar measurements and FLEXPART simulations

Figure 3 (solid lines) shows the backscatter coefficient (β) profiles at 355 nm retrieved from lidar measurements performed from 20 April until 22 April. β-profiles have been retrieved from one-hour-average lidar measurements. More specifically, the profile at 05:30 UTC was calculated by averaging lidar measurements from 05:00 to 06:00 UTC. Aerosol optical thicknesses (AOTs) at 355 nm, calculated from lidar profiles are also reported in each plot of Fig. 3. To this end, we have assumed that extinction profiles did not vary with altitude in the lowermost aerosol layer, whose height is of the order of

ACPD
12, 15301–15335, 2012

the planetary boundary layer (PBL) height (De Tomasi and Perrone, 2006). Then, we can assume that aerosol particles are well mixed within the PBL. Dotted lines in Fig. 3 represent one-hour average vertical profiles of the volcanic ash mass concentration at the lidar site from FLEXPART simulations.

Figure 3a shows that aerosol particles monitored by the lidar were mainly located below 3 km from the ground level at 5:30 UTC of 20 April. These aerosols have hardly been influenced by volcanic ash since FLEXPART shows that volcanic ash was not yet present at that time. The aerosol-load-height increased with the time of the day and the comparison of Fig. 3a, b shows that at 17:30 UTC, backscatter coefficients were characterized by larger values mainly within the 2.5–3.5 km altitude range, for which FLEXPART predicts the arrival of ash. So, it is likely that the advection of volcanic aerosol has significantly contributed to the increase of β values above 2.5 km from the ground level. The simulated volcanic ash was mainly located between 2.5–3.5 km above the ground level (a.g.l.) at 17:30 UTC (Fig. 3b, dotted line) and the simulated concentrations at this altitude have increased by orders of magnitude six hours later (Fig. 3c, dotted line). Extinction (α) and lidar ratio (LR) profiles retrieved from nighttime Raman lidar measurements (De Tomasi et al., 2006) are plotted in Fig. 4. The lidar ratio profile at 19:30 UTC of 20 April (Fig. 4a, dots) allows inferring two main aerosol layers: one extends up to about 2 km above ground level and is characterized by LRs $\cong$45 sr, and the other extends over the 2.5–3.5 km range and is characterized by lidar ratios spanning the 65–71 sr range. We believe that the upper aerosol layer (Fig. 4a, dots), characterized by larger lidar ratios, has been quite affected by volcanic aerosol. This comment is supported by the time evolution of the simulated volcanic ash (Fig. 3, dotted lines) and by the measurements performed over Greece and Turkey by Papayannis et al. (2012), who reported lidar ratios at 355 nm of 55–76 sr in volcanic aerosol layers 2.0–4.8 km a.g.l., in accordance with the results of this study. Aerosol particles up to about 4.5 km a.g.l. have been detected by the lidar at 23:30 UTC (Figs. 3c and 4b). Accordingly, the FLEXPART profile at 23:30 UTC (Fig. 3c) shows that the volcanic ash extends up to 6 km a.g.l. The highest concentrations of about 170 $\mu g\,m^{-3}$ at ~3 km a.g.l.

ACPD
12, 15301–15335, 2012

are about a factor 7 lower than the highest values simulated on 16 April over Leipzig. This suggests that the volcanic ash over Southeastern Italy was strongly diluted. Notice that on 16 April, Asmann et al. (2010) found from lidar measurements at 355 nm performed over Leipzig, that backscatter and extinction coefficients reached peak values of 7.5 $Mm^{-1} sr^{-1}$ and 370 Mm^{-1}, respectively in the center of the ash plume located from ~2.7 up to ~4.2 km a.g.l. Figure 3b (solid line) and Fig. 4b (solid line) of this study show that at 23:30 UTC of 20 April backscatter and extinction coefficients varied up to 0.7 $Mm^{-1} sr^{-1}$ and 30 Mm^{-1}, respectively, within 3–4 km a.g.l. If we assume that the aerosol load located above 3 km from the ground was mainly due to volcanic aerosol in accordance with the above reported discussion, we obtain that extinction and backscatter coefficients mainly due to volcanic aerosol were over Lecce about a factor 10 lower than the highest values monitored at Leipzig on 16 April. These last findings which are in reasonable accordance with FLEXPART results relating peak ash levels at Leipzig (16 April) and Lecce (20 April), further more support the arrival of dilute ash over Lecce. Notice that the comparison of Fig. 3a, c indicates that non-volcanic, pre-existing particles were mainly responsible for the larger backscatter and extinction coefficients retrieved below 3 km from the ground level.

Lidar ratio profiles plotted in Fig. 4b, c (dots) show that LR values spanned the 38–60 sr range below 3 km and were less dependent on altitude at 23:30 UTC of 20 April and at 02:30 of 21 April than for the earlier measurements. The mixing of volcanic aerosols with underlying aerosol particles as a consequence of sedimentation processes and/or the advection of volcanic aerosol also at lower altitudes were likely responsible for this result. FLEXPART numerical simulations show that volcanic ash also arrived at lower altitudes for the later profiles (Fig. 3c, d, dotted lines).

The aerosol load and the maximum height where aerosols have been detected by the lidar decreased with time on 21 April. These results are due to both the lower contribution of volcanic aerosols (Fig. 3) as FLEXPART volcanic ash profiles indicate, and the lower contribution of non-volcanic particles mainly located up to about 3 km a.g.l. Figure 3g (dotted line) shows that the simulated volcanic ash was mainly located from the

ACPD
12, 15301–15335, 2012

ground up to ∼1.2 km and from 2 up to ∼3.7 km at 23:30 UTC of 21 April, in satisfactory accordance with lidar measurements which detected aerosol particles up to ∼3.7 km a.g.l. (Fig. 3g, solid line). Aerosol particles were located up to ∼3.2 km a.g.l. and lidar ratios spanned the 32–50 sr range at 02:30 UTC of 22 April (Figs. 3g and 4d). Then, both the backscatter coefficient values (solid line) and the simulated volcanic ash mass concentrations (dotted line) were characterized by rather low values at 17.30 UTC of 22 April (Fig. 3l). One must be aware that volcanic ash mass concentration profiles from FLEXPART cannot be directly compared to lidar profiles, since FLEXPART profiles are only representative of volcanic ash particles, while non-volcanic particles have also contributed to the retrieved lidar profiles of Fig. 3 mainly up to about 3 km a.g.l. However, FLEXPART simulations have allowed to clearly identifying the volcanic aerosol impact at the lidar site, in accordance with the above reported discussion.

Figure 5 shows the time evolution from 20 to 22 April 2010 of the ash total column mass concentration from FLEXPART (Ma, full triangles) above the lidar site and the aerosol optical thickness at 355 nm (open dots) retrieved from lidar measurements. The time evolution of the AOT is similar to that of the ash total column mass concentration mainly after midday of 21 April. AOTs are quite dependent on aerosol optical and microphysical properties. So, the similarity between the AOT and the Ma time evolution (Fig. 5) likely indicates that the contribution of volcanic particles all over the aerosol column was more significant since midday of 21 April. Volcanic ash, lidar and lidar ratio profiles (Fig. 4, full dots) support last comment, as it is demonstrated below. The comparison of Fig. 3a and 3b reveals that non-volcanic aerosols located up to 3 km a.g.l. were mainly responsible for the rather high AOTs retrieved from lidar measurements performed on the day hours of 20 April. Then, the comparison of Fig. 3c and 3b shows that the aerosol load up to ∼1.5 km a.g.l., which is mainly due to non-volcanic aerosol, has decreased on the night of 20–21 April as AOT values ∼0.3 demonstrate (Fig. 5). A significant increase of the aerosol load leading to AOTs ≅0.4 was detected by the lidar within 14:00–16:00 UTC of 21 April (Fig. 5). The increase of the aerosol load at altitudes within 1–3 km a.g.l. was responsible for this result, in accordance to Fig. 3e and

ACPD
12, 15301–15335, 2012

likely volcanic particles have significantly contributed to the AOT increase. FLEXPART numerical simulations show that ash concentrations were larger at these altitudes and at larger altitudes. Thus, changes of the contribution by volcanic and non-volcanic particles have contributed to the larger variability of the aerosol load revealed by Fig. 3 and as a consequence, it has not been possible to obtain a proper estimate of the AOT due to volcanic particles by integrating lidar measurements and FLEXPART simulations.

3.3 AERONET sun/sky photometer measurements and FLEXPART simulations

The AERONET values of the AOT at 340 nm (Version 2, Level 2 data) retrieved from sun/sky photometer measurements performed from 20 to 22 April 2010 are plotted in Fig. 5 (full circles). We observe that the few available AERONET-AOTs at 340 nm are in satisfactory agreement with lidar AOTs at 355 nm. Figure 6 shows the evolution with time of the AOT at 500 nm (full dots) and the fine mode fraction η (open triangles) from 20 to 22 April (SDA Version 4.1, Level 2 data). η represents the ratio of the AOT by fine mode particles (particles with a radius r smaller than 0.4–0.5 µm) to the AOT by all aerosol particles. Figure 6 shows that AOT (550 nm) values decrease from 20 to 22 April, in accordance with lidar-AOT (355 nm) values. The fine mode fraction also decrease from 20 to 22 April (Fig. 6, open triangles), indicating that the contribution of coarse mode particles increases from 20 to 22 April. The columnar volume size distribution profiles retrieved on 20 and 21 April, from AERONET sun/sky photometer measurements are plotted in Fig. 7a, b. No data are available for 19 and 22 April. The volume size distributions retrieved on 20 April at 14:15 and 15:45 UTC are probably not or only weakly affected by the contribution of volcanic aerosols, as discussed previously. If we assume that the aerosols monitored on 21 April have been affected by the contribution of volcanic ash, we can use the differences ($\Delta(\mathrm{d}V(r)/\mathrm{d}\ln r)$) between the volume size distribution retrieved, for instance on 21 April at 14:49 UTC, and the one retrieved on 20 April at 14:15 UTC, to determine the size distribution of volcanic aerosols. Figure 8 (solid line) shows the mass size distribution calculated in accordance with the

ACPD
12, 15301–15335, 2012

following relationship:

$$\Delta\left(\frac{\mathrm{d}M}{\mathrm{d}\log(r)}\right) = \Delta\left(\frac{\mathrm{d}V(r)}{\mathrm{d}\ln r}\right)\cdot\ln 10\cdot\rho$$

where $\rho = 3.0\,\mathrm{g\,cm^{-3}}$ represents the particle density for volcanic aerosol, according to Kristiansen et al. (2012). Positive $\Delta(\mathrm{d}M/\mathrm{d}\log(r))$ values are found for the 0.05–0.11 µm radius range and for radii $r > 0.5\,\mu\mathrm{m}$ (Fig. 8, solid line). While the difference for the small radii could be explained by the nucleation and subsequent growth of sulphate particles from volcanic SO_2 emissions, the difference for particles with radius $r > 0.5\,\mu\mathrm{m}$ are very likely due to coarse volcanic ash particles. This result is consistent with measurements performed over Central Europe (e.g., Emeis et al., 2010; Petaja et al., 2012). A drastic increase of particles with diameter greater than 1 µm was observed at Augsburg, Germany, during the volcanic ash plume impact episode (Pitz et al., 2001). Moreover, size distribution measurements during aircraft flights over Central Europe also revealed the dominance of coarse particles to the total particulate mass in the volcanic ash plume, in accordance with mass size distributions by FLEXPART simulations (e.g., Kristiansen et al., 2012). Notice that most of the accumulation mode aerosols, which are typical for aged aerosol originating from anthropogenic emissions, are deficient in the later observation. The FLEXPART mass size distributions ($\mathrm{d}M/\mathrm{d}\log(r)$) for the monitoring site of this study are plotted in Fig. 9a–c for selected day hours of 20, 21, and 22 April. The particle density is assumed to be $3.0\,\mathrm{g\,cm^{-3}}$. Mass size distribution profiles of Fig. 9 represent 1-h-average profiles. Please note that the $\mathrm{d}M/\mathrm{d}\log(r)$ data points of the 20 April profile at 23:30 UTC (Fig. 8a) must be multiplied by a factor 2: volcanic ash mass concentrations reached the highest values on the night of 20 April over Southeastern Italy, in accordance with FLEXPART simulations (Figs. 2, 3). We observe from Fig. 9 that modeled mass size distributions are dominated by particles with radius $r > 1\,\mu\mathrm{m}$. Dotted and dashed lines in Fig. 8 show for comparison the FLEXPART mass size distributions referring to 11:30 and 14:30 UTC, respectively of 21 April. Hence, experimentally determined $\Delta(\mathrm{d}M/\mathrm{d}\log(r))$ values are in reasonable agreement with FLEXPART

ACPD
12, 15301–15335, 2012

mass size distributions. FLEXPART particle size distributions cannot be directly compared to AERONET columnar volume size distributions, since non-volcanic particles as well as sulphate particles of volcanic origin may have contributed to the retrieved AERONET profiles, while FLEXPART profiles are only representative of volcanic ash particles.

It is worth noting from Fig. 9 that the modeled mass size distributions of 22 April (Fig. 8c) are shifted to larger particle sizes than the ones of 20 April (Fig. 8a). This result is in accordance with both the AERONET fine-mode-fraction means which have decreased from 20 to 22 April (Fig. 6, open triangles) and the ground measurements of size segregated mass concentrations, as it will be shown in the following paragraph. In conclusion, we believe that the integrated use of FLEXPART simulations and sun/sky photometer measurements has allowed us to clearly identify the volcanic aerosol impact on columnar volume size distributions retrieved from sun/sky photometer measurements and to estimate the mass size distribution of the advected volcanic aerosol.

3.4 In-situ measurements

Figure 7c shows the volume size distributions from TSI-APS (3321) measurements performed at the lidar site (~10 m a.g.l.) on 21 April at 14:49 and 16:11 UTC, respectively. The comparison of Fig. 7b, c reveals that the size distributions near the ground were similar to the columnar size distributions retrieved from AERONET sun-sky photometer measurements at the same time. In both cases, there is a minimum at about 0.4–0.5 µm and a coarse mode peak at about 1.5–2.0 µm. In addition, the volume concentration of both the column-integrated and the ground-based distribution was larger at 16:11 than at 14:49 UTC. Hence, the significant contribution of particles with radius $r > 1$ µm revealed by Fig. 7c was likely due to the impact of volcanic aerosol at ground. This is in agreement with the fact that lidar ratios were enhanced down into the boundary layer on 21 April and also agrees with the FLEXPART simulations, which show presence of volcanic ash in the boundary layer, albeit at lower concentrations than aloft. In situ measurements performed by Lettino et al. (2012) over Southern Italy and

ACPD
12, 15301–15335, 2012

by Rossini et al. (2012) over Central Italy have also revealed the impact at the ground of volcanic particles with radius $r > 1\,\mu m$.

PM_1 (particles with the aerodynamic diameter $\leq 1\,\mu m$) and $PM_{2.5}$ (particles with the aerodynamic diameter $\leq 2.5\,\mu m$) samples have also been collected at the lidar site from 21 to 24 April. Mass concentrations of daily PM_1 and $PM_{2.5}$ samples revealed that the $PM_1/PM_{2.5}$ mass ratios were 0.69, 0.66, and 0.60 on 20, 21, and 22 April, respectively, indicating that the contribution of particles with radius $>0.5\,\mu m$ increased from 21 to 22 April, in accordance with the daily evolution of the AERONET fine mode fraction.

In-situ SO_2 and PM_{10} measurements performed by the Regional Air Quality Agency have been analyzed to infer the volcanic aerosol effects on regional scale. Enhanced PM_{10} and SO_2 concentrations were monitored all over Southeastern Italy from 20 up to 22 April 2010, in accordance with measurements by the Regional Air Quality Agency (www.arpa.puglia.it/web/guest/qariainq) of Apulia Region. Table 1 shows the daily PM_{10} mass concentrations monitored from 19 up to 23 April 2010, at 10 selected sites of the 400 km long Apulia Region (Fig. 10) in addition to the average value (avg) over all sites. Uncertainties of PM_{10} levels are smaller than 5 %. It seems likely from Table 1 that the larger PM_{10} mass concentrations monitored on 21 and/or 22 April have mainly been caused by the volcanic aerosol impact and not by other regional and/or local aerosol sources. PM_{10} levels of sites differently affected by local pollution (e.g. urban, sub-urban, rural, and background sites) have been reported in Table 1. Enhanced PM_{10} mass concentrations were found all over Europe for the impact of the volcanic aerosol (e.g., Emeis et al., 2011). Moreover, meteorological synoptic maps, analytical back trajectories (Fig. 1), and FLEXPART simulations (Fig. 2) all support a regional-scale impact.

Figure 11 shows the volcanic ash mass concentrations ($\mu g\,m^{-3}$) from FLEXPART simulations at 150 m a.g.l. at the lidar site. Daily means of the volcanic ash mass concentration were 0.7, 4.5, and 3.8 $\mu g\,m^{-3}$ on 20, 21, and 22 April, respectively. Site I daily PM_{10} levels and daily PM_{10} mass concentrations averaged over all sites (Table 1) are also reported in Fig. 11 by dotted and dashed lines, respectively. At site I, only

ACPD
12, 15301–15335, 2012

a few hundred meters away from the lidar monitoring site, the daily levels of PM_{10} were on 20, 21, and 22 April, 4, 6, and 5 $\mu g\,m^{-3}$, respectively larger than the daily mean on 19 April, a day not yet affected by volcanic particles (Table 1). These enhancements are quite consistent with the values simulated by FLEXPART. Sites H and Site L are only a few tens of kilometres away from the lidar site (Fig. 11) and Table 1 shows that the enhancements of the PM_{10} levels on 20, 21, and 22 April, respectively, are at both sites rather similar to those observed at Site I. Finally, Table 1 and Fig. 11 (dashed line) shows that the daily PM_{10} mean levels were on 20, 21, and 22 April, 4, 9, and 5 $\mu g\,m^{-3}$, respectively larger than the daily PM_{10} mean level on 19 April. Figure 12 shows the time series of PM_{10} and SO_2 mass concentrations at sites C and G (Fig. 10) which are approximately one hundred and two hundred kms away from the monitoring site of this study. The correlation between PM_{10} and SO_2 mass concentrations, especially at site C, is also suggestive of a volcanic source of the PM_{10} enhancements, since SO_2 is also emitted by the volcano. Correlations between particulate matter and SO_2 in the Eyjafjallajökull plume have been observed earlier both by aircraft (Schumann et al., 2010) as well as at the ground (e.g., Emeis et al., 2011).

4 Summary and conclusion

Results of the characterization of aged volcanic aerosol by lidar, sun/sky photometer, and in-situ measurements at a south eastern Italian site, which is approximately 4000 km away from the Eyjfjallajökull volcano, have been reported. Meteorological synoptic maps, analytical back trajectories and numerical simulations by the FLEXPART dispersion model indicate that Southern Italy was affected by volcanic ash particles from 20 up to 22 April, 2010. However, both the peak concentrations as well as the total column loadings of volcanic ash simulated by FLEXPART were about one order of magnitude lower than corresponding values simulated over Central Europe on 16 April. This suggests that the volcanic ash over Southeastern Italy was strongly diluted. Lidar measurements performed at the Physics Department of the University of Salento

ACPD
12, 15301–15335, 2012

(40.4° N; 18.1° E) within EARLINET (European Aerosol Research LIdar NETwork EARLINET) have shown that at 18:30 UTC of 20 April, volcanic ash particles were located near 2.5–3.5 km above ground level. Lidar ratios (LRs) at 355 nm were about 65–71 sr inside the volcanic aerosol layer, but only about 45 sr at lower altitudes. The dependence of LR values on altitude decreased with time as ash also arrived in the boundary layer (as also simulated ash profiles by FLEXPART), but the vertical structure of the lidar backscatter coefficient still varied significantly on 20, 21, and 22 April for the high variability of the contribution of both the volcanic and non-volcanic particles. We have also found that the time series of the aerosol optical depth by lidar measurements were similar to the simulated ash-total-column mass concentration after midday of 21 April likely for the more significant contribution of volcanic particles to the whole aerosol load.

AERONET sun-sky photometer measurements have revealed that volcanic particles with radius $r > 0.5\,\mu m$ were mostly advected over Southeastern Italy. In fact, the estimated mass size distribution of volcanic particles from sun-sky photometer measurements was in reasonable accordance with the mass size distribution for volcanic ash by FLEXPART simulations at 14:15 UTC of 21 April. Sun-sky photometer measurements have also revealed that the contribution of coarse particles increased with time during the arrival of the volcanic ash plume. In fact, the aerosol fine mode fraction varied from 0.85 to 0.94 on 20 April, before the arrival of volcanic ash, and from 0.25 to 0.82 on 22 April, when the ash cloud had arrived. Ground-level in-situ measurements of the aerosol size distribution were also in satisfactory accordance with columnar-average size distributions from sun/sky photometer measurements and with size segregated measurements of ground PM mass concentrations. Daily PM_1 and $PM_{2.5}$ mass concentrations have shown that the $PM_1/PM_{2.5}$ ratio was 0.69, 0.66, and 0.60 on 20, 21, and 22 April, again suggesting the advection of volcanic particles with aerodynamic radius $r > 0.5\,\mu m$. Enhanced PM_{10} and SO_2 concentrations were also found all over a 400 km long area of Southern Italy, on 20 and/or 21 April, 2010. In particular, the

ACPD
12, 15301–15335, 2012

estimated enhancement of PM_{10} from volcanic particles was ~4, 6, and 5 $\mu g\,m^{-3}$ on 20, 21, and 22 April, respectively at the lidar site.

In conclusion, the paper has shown that the integrated use of different remote sensing and in situ sampling devices has allowed to properly characterizing optical and microphysical properties of aged volcanic particles even in a plume that was very dilute compared to Central Europe a few days earlier. The integrated use of model and experimental data was prerequisite to clearly identify signatures and impact levels of volcanic particle at a distance of 4000 km from the volcano site. Hence, the paper has also contributed to the validation of the FLEXPART dispersion model. It is rather important to implement and test advanced dispersion models to better evaluate in the future the hazard to aviation due to volcanic ash and, more generally, to better evaluate the impact of volcanic ash emissions on the environment.

Acknowledgements. The financial support of the EARLINET-ASOS Network by the European Commission under grant RICA-025991 is gratefully acknowledged.

References

Ansmann A., Riebesell, M., Wandinger, U., Weitkamp, C., Voss, E., Lahmann, W., and Michaelis, W.: Combined raman elastic-backscatter LIDAR for vertical profiling of moisture, aerosol extinction, backscatter, and LIDAR ratio, Appl. Phys., 55, 18–28, 1992.

Ansmann, A., Tesche, M., Gross, S., Freudenthaler, V., Seifert, P., Hiebsch, A., Schmidt, J., Wandinger, U., Mattis, I., and Wiegner, M.: The 16 April 2010 major volcanic ash plume over Central Europe: EARLINET lidar and AERONET photometer observations at Leipzig and Munich, Germany, Geophys. Res. Lett., 37, L13810, doi:10.1029/2010GL043809, 2010.

Bevington, P. R. and Robinson, K. D.: Data Reduction and Error Analysis for the Physical Sciences, 3rd edn., McGraw-Hill, Boston, MA, 2003.

Bukowiecki, N., Zieger, P., Weingartner, E., Jurányi, Z., Gysel, M., Neininger, B., Schneider, B., Hueglin, C., Ulrich, A., Wichser, A., Henne, S., Brunner, D., Kaegi, R., Schwikowski, M., Tobler, L., Wienhold, F. G., Engel, I., Buchmann, B., Peter, T., and Baltensperger, U.: Ground-based and airborne in-situ measurements of the Eyjafjallajökull volcanic aerosol plume in

ACPD

12, 15301–15335, 2012

Switzerland in spring 2010, Atmos. Chem. Phys., 11, 10011–10030, doi:10.5194/acp-11-10011-2011, 2011.
Campanelli, M., Estelles, V., Smyth, T., Tomasi, C., Martìnez-Lozano, M. P., Claxton, B., Muller, P., Pappalardo, G., Pietruczuk, A., Shanklin, J., Colwell, S., Wrench, C., Lupi, A., Mazzola, M., Lanconelli, C., Vitale, V., Congeduti, F., Dionisi, D., Cardillo, F., Cacciani, M., Casasanta, G., and Nakajima, T.: Monitoring of Eyjafjallajökull volcanic aerosol by the new European Skynet Radiometers (ESR) network, Atmos. Environ., 48, 33–45, doi:10.1016/j.atmosenv.2011.09.070, 2012.
De Tomasi, F. and Perrone, M. R.: Lidar measurements of tropospheric water vapor and aerosol profiles over South-Eastern Italy, J. Geophys. Res., 108, 4286–4297, 2003.
De Tomasi, F., Tafuro, A. M., and Perrone, M. R.: Height and seasonal dependence of aerosol optical properties over South-East Italy, J. Geophys. Res., 111, D10203, doi:10.1029/2005JD006779, 2006.
Draxler, R. R. and Rolph, G. D.: HYSPLIT (HYbrid Single-Particle Lagrangian Integrated Trajectory) Model access via NOAA ARL READY, available online: http://ready.arl.noaa.gov/HYSPLIT.php, NOAA Air Resources Laboratory, Silver Spring, MD, 2010.
Dubovik, O. and King, M. D.: A flexible inversion algorithm for retrieval of aerosol optical properties from sun and sky radiance measurements, J. Geophys. Res., 105, 20673–20696, doi:10.1029/2000JD900282, 2000.
Dubovik, O., Smirnov, A., Holben, B. N., King, M. D., Kaufman, Y. J., Eck, T. F., Slutsker, I.: Accuracy assessments of aerosol optical properties retrieved from Aerosol Robotic Network (AERONET) aun and sky radiance measurements, J. Geophys. Res., 105, 9791–9806, doi:10.1029/2000JD900040, 2000.
Emeis, S., Forkel, R., Junkermann, W., Schäfer, K., Flentje, H., Gilge, S., Fricke, W., Wiegner, M., Freudenthaler, V., Groß, S., Ries, L., Meinhardt, F., Birmili, W., Münkel, C., Obleitner, F., and Suppan, P.: Measurement and simulation of the 16/17 April 2010 Eyjafjallajökull volcanic ash layer dispersion in the northern Alpine region, Atmos. Chem. Phys., 11, 2689–2701, doi:10.5194/acp-11-2689-2011, 2011.
Folch, A., Costa, A., and Basart, S.: Validation of the FALL3D ash dispersion model using observations of the 2010 Eyjafjallajökull volcanic ash clouds, Atmos. Environ., 48, 165–183, doi:10.1016/j.atmosenv.2011.06.072, 2012.
Holben, B. N., Eck, T. F., Slutsker, I., Tanré, D., Buis, J. P., Setzer, A., Vermote, E., Reagan, J. A., Kaufman, Y. J., Nakajima, T., Lavenu, F., Jankowiak, I., and Smirnov, A.: AERONET –

ACPD
12, 15301–15335, 2012

a federate instrument network and data archive for aerosol characterization, Remote Sens. Environ. 66, 1–16, 1998.

Kristiansen, N. I., Stohl, A., Prata, A. J., Bukowiecki, N., Dacre, H., Eckhardt, S., Henne, S., Hort, M. C., Johnson, B. T., Marenco, F., Neininger, B., Reitebuch, O., Seibert, P., Thomson, D. J., Webster, H. N., and Weinzierl, B.: Performance assessment of a volcanic ash transport model mini-ensemble used for inverse modelling of the 2010 Eyjafjallajökull eruption, J. Geophys. Res., 117, D00U11, doi:10.1029/2011JD016844, 2012.

Langmann, B., Folch, A., Hensch, M., and Matthias, V.: Volcanic ash over Europe during the eruption of Eyjafjallajökull on Iceland, April–May 2010, Atmos. Environ., 48, 1–8, doi:10.1016/j.atmosenv.2011.03.054, 2012.

Lettino, A., Caggiano, R., Fiore, S., Macchiato, M., Sabia, S., and Trippetta, S.: Eyjafjallajökull volcanic ash in Southern Italy, Atmos. Environ., 48, 97–103, doi:10.1016/j.atmosenv.2011.05.037, 2012.

Madonna, F., Amodeo, A., D'Amico, G., Mona, L., and Pappalardo G.: Observation of non-spherical ultragiant aerosol using a microwave radar, Geophys. Res. Lett., 37, L21814, doi:10.1029/2010GL044999, 2010.

Matthias, V., Freudenthaler, V., Amodeo, A., Balis, D., Boesenberg, J., Chaikovsky, A., Chourdakis, G., Comeron, A., Delaval, A., De Tomasi, F., Eixmann, R., Hagard, A., Komguem, L., Kreipl, S., Matthey, R., Rizi, V., Rodrigues, J. A., Wandinger, U., and Wang, X.: Aerosol lidar intercomparison in the framework of the EARLINET project: 1. Instrument, Appl. Optics., 43, 961–976, 2004.

Mona, L., Amodeo, A., D'Amico, G., Giunta, A., Madonna, F., and Pappalardo, G.: Multi-wavelength Raman lidar observations of the Eyjafjallajökull volcanic cloud over Potenza, southern Italy, Atmos. Chem. Phys., 12, 2229–2244, doi:10.5194/acp-12-2229-2012, 2012.

Papayannis A., Mamouri R. E., Amiridis, V., Giannakaki, E., Veselovskii, I., Kokkalis, P., Tsaknakis, G., Balis, D., Kristiansen, N. I., Stohl, A., Korenskiy, M., Allaakhverdiev, K., Huseyinoglu, M. F., and Baykara, T.: Optical properties and vertical extension of aged ash layers over Eastern Mediterranean as observed by Raman lidars during Eyjafjallajökull eruption, Atmos. Environ., 48, 56–65, 2012.

Petäjä, T., Laakso, L., Grönholm, T., Launiainen, S., Evele-Peltoniemi, I., Virkkula, A., Leskinen, A., Backman, J., Manninen, H. E., Sipilä, M., Haapanala, S., Hämeri, K., Vanhala, E., Tuomi, T., Paatero, J., Aurela, M., Hakola, H., Makkonen, U., Hellén, H., Hillamo, R., Vira, J., Prank, M., Sofiev, M., Siitari-Kauppi, M., Laaksonen, A., Lehtinen, K. E. J., Kulmala, M.,

ACPD
12, 15301–15335, 2012

Viisanen, Y., and Kerminen, V.-M.: In-situ observations of Eyjafjallajökull ash particles by hot-air balloon, Atmos. Environ. 48, 104–112, doi:10.1016/j.atmosenv.2011.08.046, 2012.
Petersen, G. N.: A short meteorological overview of the Eyjafjallajökull eruption 14 April – 23 May 2010, Weather, 65, 203–207, 2010.
Pitz, M., Gu, J., Soentgen, J., Peters, A., and Cyrys, J.: Particle size distribution factor as an indicator for the impact of the Eyjafjallajökull ash plume at ground level in Augsburg, Germany, Atmos. Chem. Phys., 11, 9367–9374, doi:10.5194/acp-11-9367-2011, 2011.
Revuelta, M. A., Sastre, M., Fernández, A. J., Martín, L., García, R., Gómez-Moreno, F. J., Artíñano, B., Pujadas, M., and Molero, F.: Characterization of the Eyjafjallajökull volcanic plume over the Iberian Peninsula by lidar remote sensing and ground-level data collection, Atmos. Environ., 48, 46–55, doi:10.1016/j.atmosenv.2011.05.033, 2012.
Rossini, P., Molinaroli, E., De Falco, G., Fiesoletti, F., Papa, S., Pari, E., Renzulli, A., Tentoni, P., Testoni, A., Valentini, L., and Matteucci, G.: April–May 2010 Eyjafjallajökull volcanic fallout over Rimini, Italy, Atmos. Environ., 48, 122–128, doi:10.1016/j.atmosenv.2011.05.018, 2012.
Schumann, U., Weinzierl, B., Reitebuch, O., Schlager, H., Minikin, A., Forster, C., Baumann, R., Sailer, T., Graf, K., Mannstein, H., Voigt, C., Rahm, S., Simmet, R., Scheibe, M., Lichtenstern, M., Stock, P., Rüba, H., Schäuble, D., Tafferner, A., Rautenhaus, M., Gerz, T., Ziereis, H., Krautstrunk, M., Mallaun, C., Gayet, J.-F., Lieke, K., Kandler, K., Ebert, M., Weinbruch, S., Stohl, A., Gasteiger, J., Groß, S., Freudenthaler, V., Wiegner, M., Ansmann, A., Tesche, M., Olafsson, H., and Sturm, K.: Airborne observations of the Eyjafjalla volcano ash cloud over Europe during air space closure in April and May 2010, Atmos. Chem. Phys., 11, 2245–2279, doi:10.5194/acp-11-2245-2011, 2011.
Smirnov, A., Holben, B. N., Eck, T. F., Dubovik, O., and Slutsker, I.: Cloud screening and quality control algorithms for the AERONET database, Remote Sens. Environ., 73, 337–349, 2000.
Stohl, A.: Computation, accuracy and application of trajectories-a review and bibliography, Atmos. Environ., 32, 947–966, 1998.
Stohl, A., Forster, C., Frank, A., Seibert, P., and Wotawa, G.: Technical note: The Lagrangian particle dispersion model FLEXPART version 6.2, Atmos. Chem. Phys., 5, 2461–2474, doi:10.5194/acp-5-2461-2005, 2005.
Stohl, A., Prata, A. J., Eckhardt, S., Clarisse, L., Durant, A., Henne, S., Kristiansen, N. I., Minikin, A., Schumann, U., Seibert, P., Stebel, K., Thomas, H. E., Thorsteinsson, T., Tørseth, K., and Weinzierl, B.: Determination of time- and height-resolved volcanic ash

ACPD
12, 15301–15335, 2012

emissions and their use for quantitative ash dispersion modeling: the 2010 Eyjafjallajökull eruption, Atmos. Chem. Phys., 11, 4333–4351, doi:10.5194/acp-11-4333-2011, 2011.

Toledano, C., Bennouna, Y., Cachorro, V., Ortiz de Galisteo, J. P., Stohl, A., Stebel, K., Kristiansen, N. I., Olmo, F. J., Lyamani, H., Obregón, M. A., Estellés, V., Wagner, F., Baldasano, J. M., González-Castanedo, V., Clarisse, L., and de Frutos, A. M.: Aerosol properties of the Eyjafjallajökull ash derived from sun photometer and satellite observations over the Iberian Peninsula, Atmos. Environ., 48, 22–32, doi:10.1016/j.atmosenv.2011.09.072, 2012.

ACPD

12, 15301–15335, 2012

Table 1. PM_{10} mass concentrations ($\mu g\,m^{-3}$) measured at selected sites in the Apulia region (shown in Fig. 10) from 19 to 23 April 2010.

Site	19 Apr ($\mu g\,m^{-3}$)	20 Apr ($\mu g\,m^{-3}$)	21 Apr ($\mu g\,m^{-3}$)	22 Apr ($\mu g\,m^{-3}$)	23 Apr ($\mu g\,m^{-3}$)
A	26	33	28	22	20
B	15	20	27	21	21
C	23	23	44	26	36
D	20	24	27	24	21
E	18	21	24	24	20
F	13	21	25	25	19
G	12	17	25	20	20
H	18	19	24	25	22
I	18	22	24	23	19
L	15	18	20	20	19
Avg	18	22	27	23	22

ACPD
12, 15301–15335, 2012

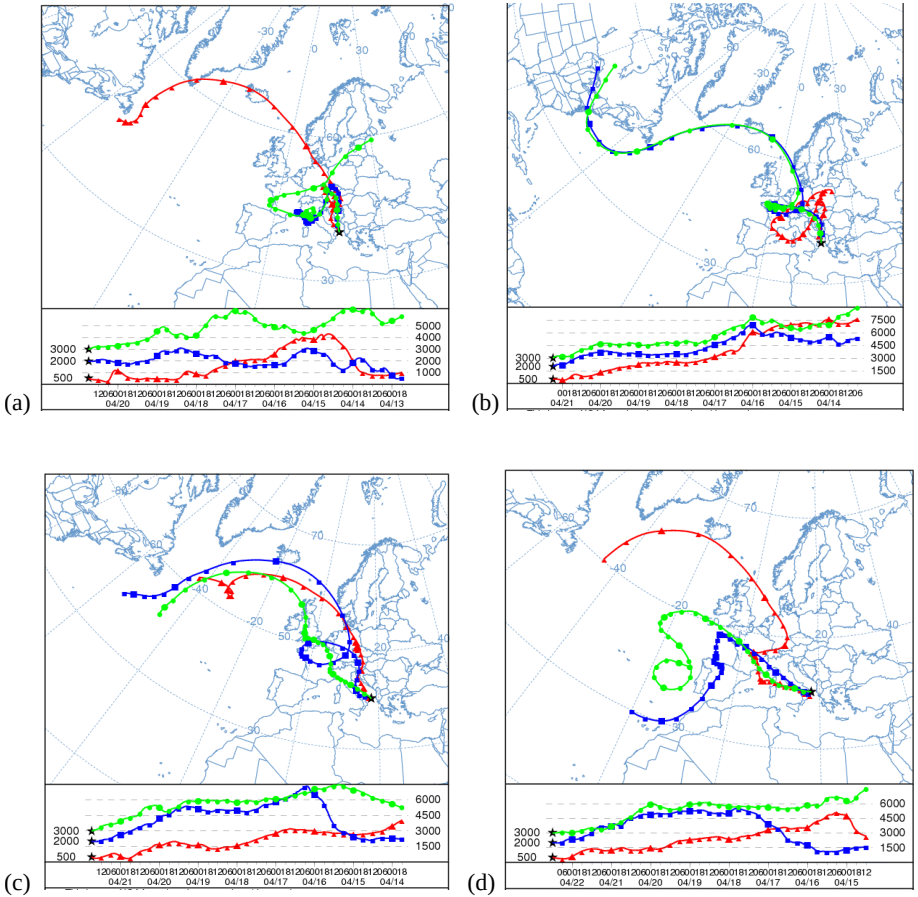

Fig. 1. 8-day back trajectories of air masses ending at the Physics Department of the Salento University, Lecce (Italy), **(a)** on 20 April at 17:30 UTC, **(b)** on 21 April at 05:30 UTC, **(c)** on 21 April at 17:30 UTC, and **(d)** on 22 April at 12:00 UTC.

ACPD
12, 15301–15335, 2012

Characterization of Eyjafjallajökull volcanic aerosols over Italy

M. R. Perrone et al.

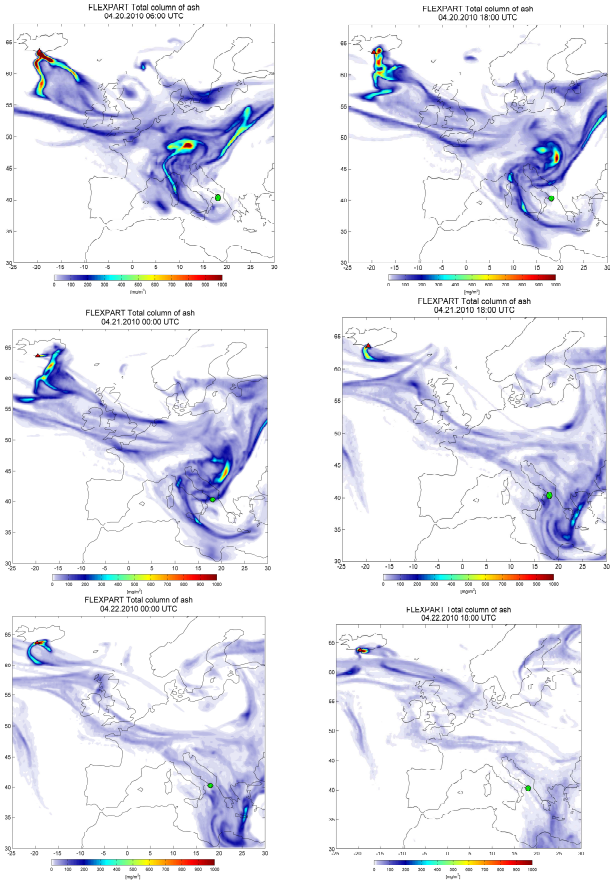

Fig. 2. FLEXPART simulations of the Eyjafjallajökull volcanic ash (total atmospheric columns in $mg\,m^{-2}$, integrated over all 25 particle size classes) at selected hours on **(a–c)** 20 April, **(d, e)** 21 April, and **(f)** 22 April. The green dot marks the monitoring site.

ACPD
12, 15301–15335, 2012

Characterization of Eyjafjallajökull volcanic aerosols over Italy

M. R. Perrone et al.

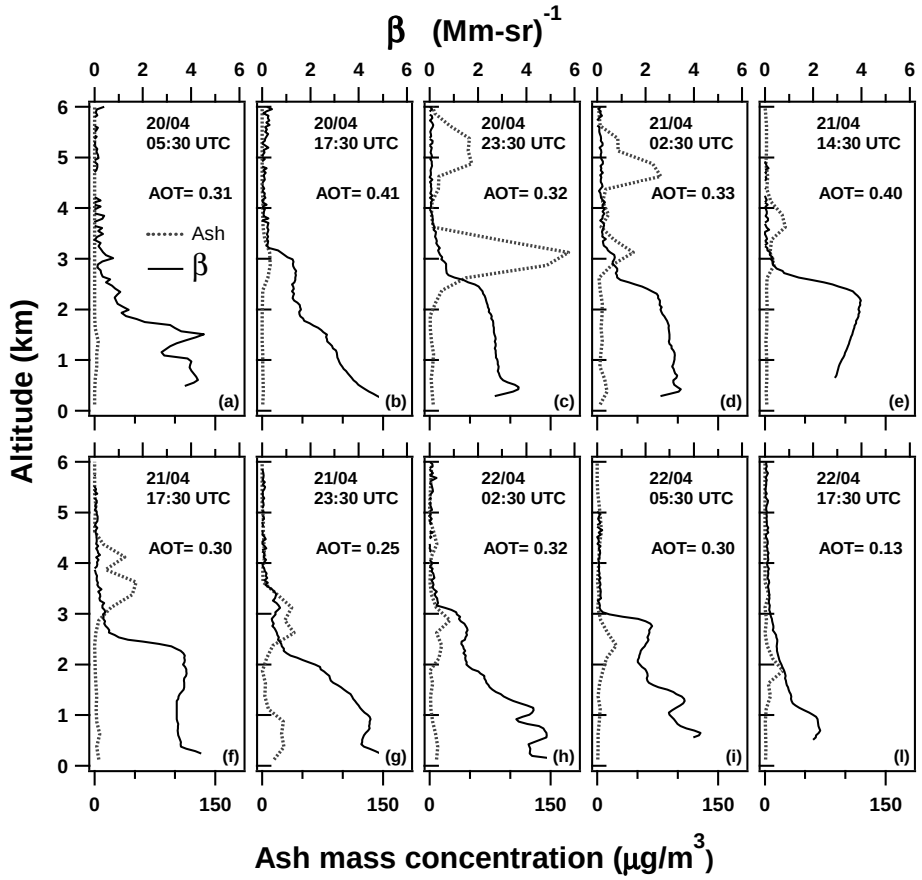

Fig. 3. Vertical profiles of the aerosol backscatter coefficient at 355 nm (solid line) and of the volcanic ash mass concentration simulated by FLEXPART (dotted line) at selected hours on 20, 21, and 22 April 2010.

ACPD
12, 15301–15335, 2012

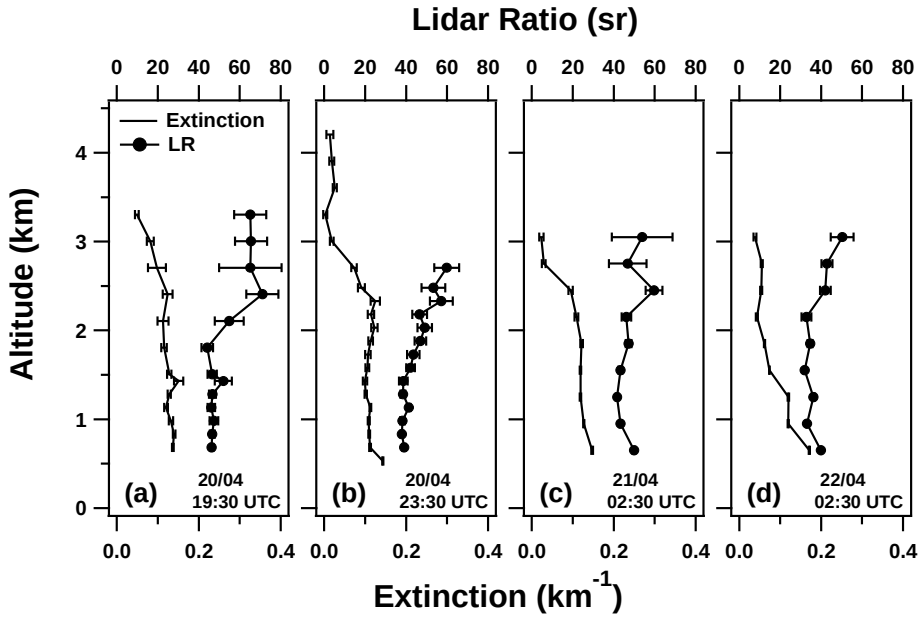

Fig. 4. Vertical profiles of the aerosol extinction coefficient and of the lidar ratio (full dots) retrieved from nighttimes lidar measurements at selected hours on 20, 21, and 22 April 2010.

ACPD
12, 15301–15335, 2012

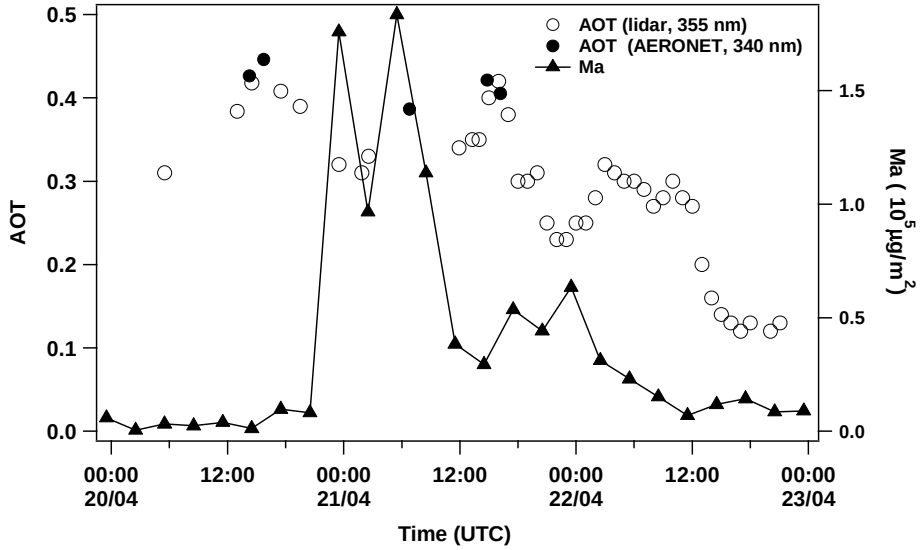

Fig. 5. Time series of the aerosol optical thickness at 355 nm from lidar measurements (open dots) and of the ash total column simulated by FLEXPART at the lidar site (full triangles). Full dots represent the aerosol optical thickness at 340 nm from AERONET sun/sky photometer measurements.

ACPD
12, 15301–15335, 2012

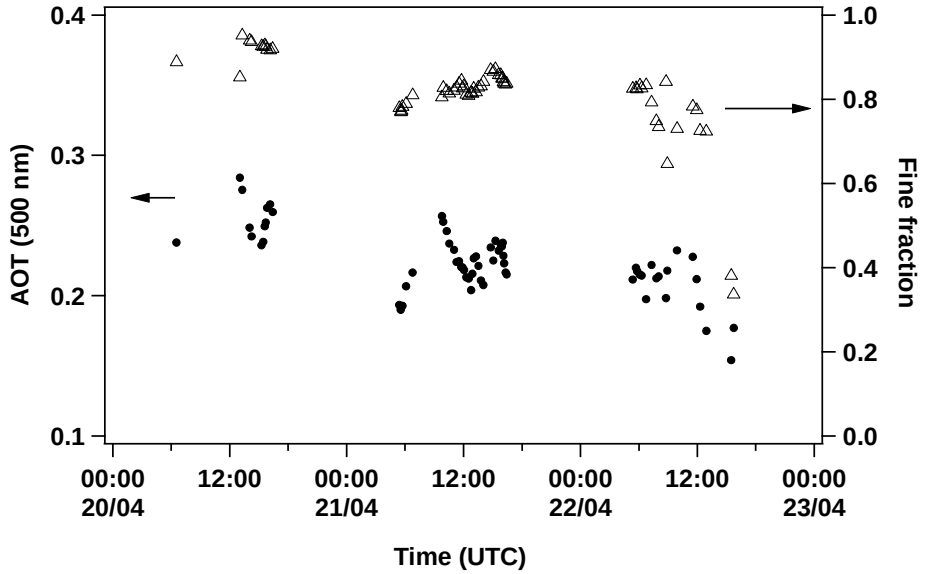

Fig. 6. Time evolution from 20 to 22 April 2010 of the aerosol optical thickness (AOT) at 500 nm (full dots) and of the fine mode fraction (open triangles) from AERONET sun/sky photometer measurements.

ACPD
12, 15301–15335, 2012

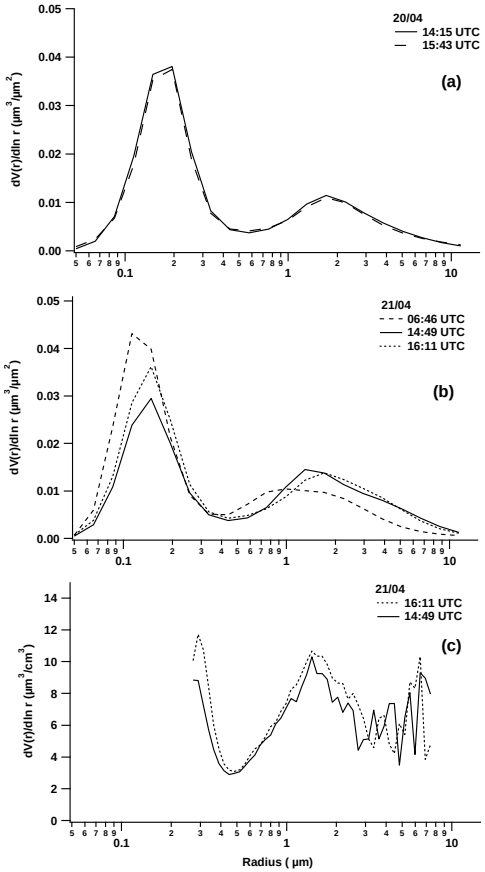

Fig. 7. Volume size distributions retrieved from AERONET sun/sky photometer measurements performed at different day hours of **(a)** 20 and **(b)** 21 April 2010. **(c)** Volume size distributions retrieved at the ground level from Aerodynamic Particle Sizer (APS 3321, TSI) measurements performed on 21 April 2010 at different day hours.

ACPD
12, 15301–15335, 2012

Characterization of Eyjafjallajökull volcanic aerosols over Italy

M. R. Perrone et al.

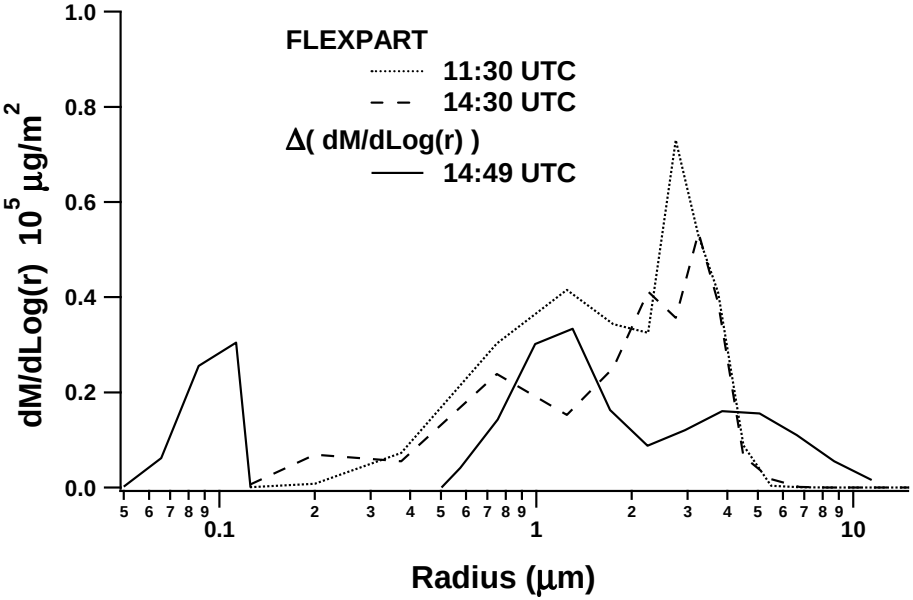

Fig. 8. Columnar mass size distribution of volcanic particles inferred from the AERONET volume size distribution retrieved at 14:49 UTC of 21 April, by setting the particle mass density for volcanic particles $\rho = 3.0\,\mathrm{g\,cm^{-3}}$ (solid line). Columnar mass size distribution of volcanic ash from FLEXPART simulations at 11:30 UTC (dotted line) and 14:30 UTC (dashed line) of 21 April 2010.

ACPD
12, 15301–15335, 2012

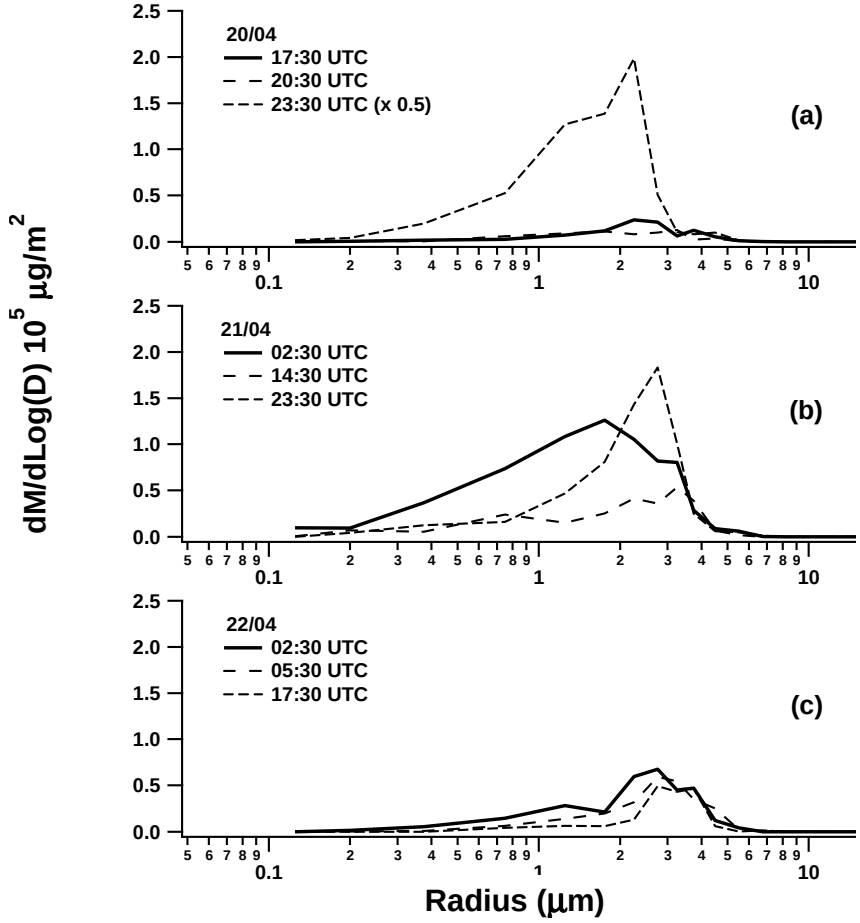

Fig. 9. Columnar mass size distribution of volcanic ash from FLEXPART simulations at selected hours on **(a)** 20, **(b)** 21, and **(c)** 22 April 2010.

ACPD
12, 15301–15335, 2012

Characterization of Eyjafjallajökull volcanic aerosols over Italy

M. R. Perrone et al.

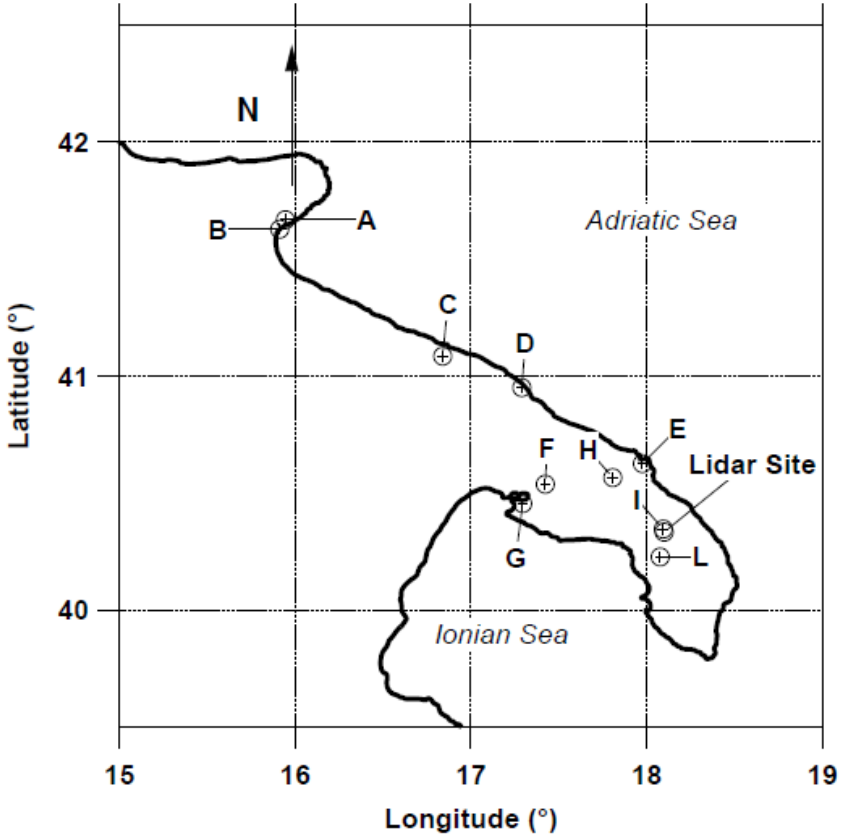

Fig. 10. Geographical locations of selected sites of the Air Quality Agency of the Apulia Region in Southeastern Italy and of the lidar site.

ACPD
12, 15301–15335, 2012

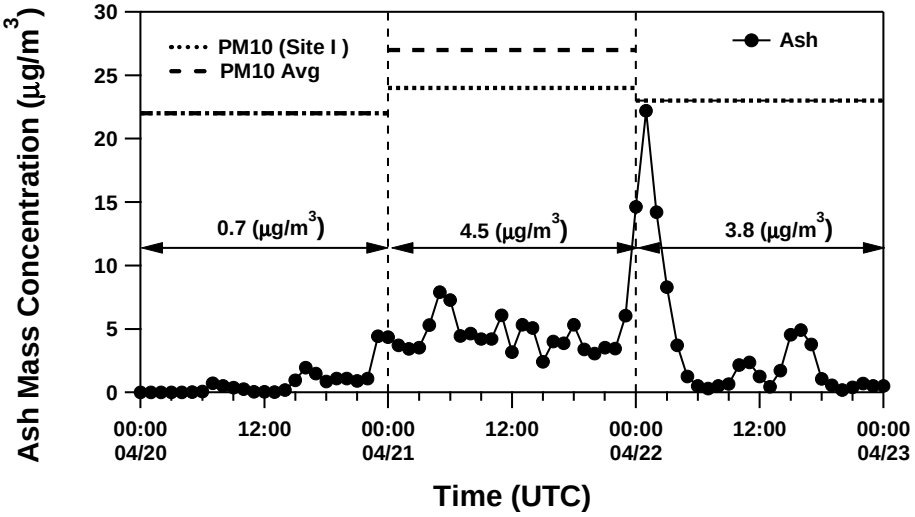

Fig. 11. Time evolution at the lidar site of the volcanic ash mass concentration ($\mu g\,m^{-3}$) at 150 m a.g.l. from FLEXPART simulations.

ACPD
12, 15301–15335, 2012

Characterization of Eyjafjallajökull volcanic aerosols over Italy

M. R. Perrone et al.

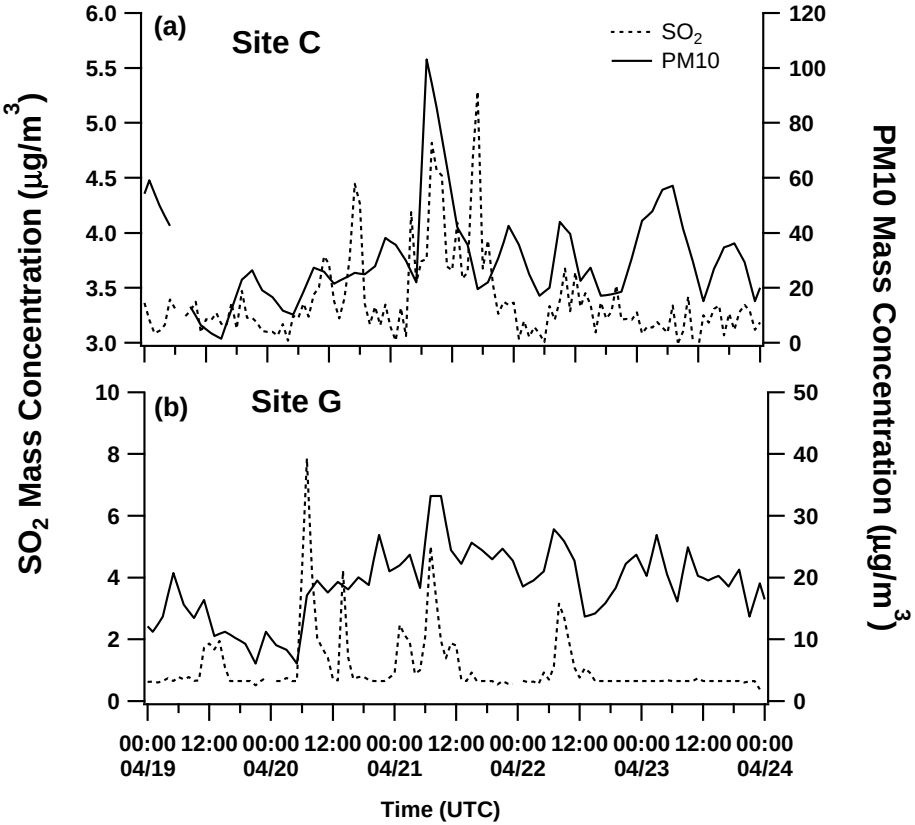

Fig. 12. Time series of PM_{10} and SO_2 mass concentrations at sites C and G (locations are shown in Fig. 10).

ACPD
12, 15301–15335, 2012